Identifying Hyper-Viscoelastic Model Parameters from an Inflation-Extension Test and Ultrasound Images

E.-J. Courtial[1,2,3] · M. Orkisz[2] · P.C. Douek[4] · L. Huet[5] · R. Fulchiron[5]

Abstract The aim of the present study was to develop and validate a method based on medical imaging to identify the parameters of a hyper-viscoelastic model suitable for describing the mechanical behavior of vascular tissues, focusing on the aorta. The method uses an inflation-extension test, and the model comprises one hyperelastic element in parallel with one or more Maxwell elements. Cylindrical samples of elastomeric silicone materials with a mechanical behavior similar to vascular tissues were placed in a circuit simulating hemodynamic flow through adequate controlled-pressure variation. Ultrasound B-mode image sequences were analyzed to measure the cyclic circumferential and longitudinal elongations. Precautions were taken *a posteriori* to resynchronize pressure and deformation signals, and thus minimize errors in the viscosity parameters estimated. The hyper-viscoelastic parameters of the samples were identified with reasonable accuracy as compared with the values obtained via standard measurements, namely tensile tests and dynamic mechanical analysis. However, the estimates of the viscosity parameters can be hampered in the case of stiffer samples. This limitation is bound to a restricted range of frequencies analyzed by the test, which mainly depends on the image acquisition rate. The use of the present method in the clinical environment for *in vivo* experiments can be foreseen provided that the local pressure measurements are available.

Keywords Inflation-extension test · Hyper-viscoelasticity · Silicone · Aortic mechanics · Vascular phantom

✉ R. Fulchiron
rene.fulchiron@univ-lyon1.fr

E.-J. Courtial
courtial@creatis.insa-lyon.fr

M. Orkisz
maciej.orkisz@creatis.insa-lyon.fr

P. C. Douek
philippe.douek@creatis.univ-lyon1.fr

L. Huet
laurent.huet@segula.fr

1 Ingénierie des Matériaux Polymères - UMR CNRS 5223, Université de Lyon - Université Lyon 1, Bâtiment POLYTECH Lyon - 15 boulevard Latarjet, Villeurbanne 69622, France

2 Université de Lyon, CREATIS; CNRS UMR 5220; Inserm U1044; INSA-Lyon; Université Lyon 1, Villeurbanne, France

3 Département recherche et innovation, SEGULA MATRA TECHNOLOGIES, Bron, France

4 Université de Lyon, CREATIS; CNRS UMR 5220; Inserm U1044; INSA-Lyon; Université Lyon 1; Hospices Civils de Lyon, Lyon, France

5 Ingénierie des Matériaux Polymères - UMR CNRS 5223, Université de Lyon - Université Lyon 1, Bâtiment POLYTECH Lyon - 15 boulevard Latarjet, Villeurbanne 69622, France

Introduction

Vascular pathologies have a direct effect on the mechanical properties of the vessel wall, mainly located in the diseased area. The methods used to describe these properties and identify their parameters contribute to fundamental advances in the field of cardiovascular radiology and surgery. They allow clinicians and researchers to predict events such as aneurysm rupture [1] and the development of diseases such as atherosclerosis [2], to describe the vascular microstructure [3, 4], as well as to create biocompatible implants for vascular reconstruction [5] or synthetic replicas [6, 7], called "phantoms," for clinicians' preoperative training in usual or innovative surgical and radiological interventions [8].

However, the assessment of mechanical behavior is often challenging because it can only be characterized through indirect measurements. Experimentally, current techniques based on medical imaging, such as magnetic resonance imaging (MRI) [9], ultrasound (US) imaging [3, 1] and X-ray computed tomography (CT) [10] are used. These techniques contribute more or less accurate data on vascular wall motion according to their spatial and temporal resolution, with the result that the parameters identified can be affected by this resolution as well as by acquisition artifacts. Owing to these uncertainties, simplified linear constitutive equations are often considered based on *in-vivo* experiments, leading to parameters such as Young's modulus [11], compliance [1] and distensibility [12, 9]. Nevertheless, studies from *in vivo* as well as *ex vivo* experiments have demonstrated that the actual vascular mechanical behavior is more complex. Indeed, in the case of the aorta tree, a nonlinear and reversible [3, 13, 14] behavior (hyperelasticity) with a phase shift between strain and stress, displaying a viscoelastic effect [15–18], has to be considered. The studies on the mechanical modeling of various vascular walls have used constitutive models that are able to predict either hyperelasticity or viscoelasticity, but the combination of both behaviors is seldom taken into account [16]. This can lead to a model inadequately describing the actual inflation and extension of the blood vessels. Indeed, longitudinal elongation is commonly overlooked in mechanical modeling [16, 3], but this approximation is not really justified, according to a recent study [19]. The identification of more realistic constitutive equations, and of the related material parameters, is a major challenge within the issues related to cardiovascular surgery.

Hence, the aim of the present study was to develop and validate a method based on medical imaging to identify the parameters of a hyper-viscoelastic model suitable for describing the mechanical behavior of vascular tissues, focusing on the aorta. This model comprises one hyperelastic element in parallel with one or more Maxwell elements. The proposed method to identify the hyper-viscoelastic model parameters was validated by applying the method to specific silicone materials and comparing the estimated parameters to reference values obtained by means of precise mechanical measurements such as uniaxial tensile and/or compression tests. This type of system has already been used in dynamic conditions to study flow [20–22] and to develop methods for disease prediction, but not for rigorous modeling of the hyper-viscoelastic behavior. The silicone samples, connected to this test bench, were subjected to various automatically controlled pressure cycles, in order to measure the induced elongation by means of ultrasound imaging.

This paper is organized as follows. The first section describes the materials used to validate the Inflation-Extension (I-E) test proposed. Then constitutive models are introduced in the second section, in which hyper-viscoelastic mechanical behavior is described. The third section deals with the experimental setup and also describes the experimental process and parameter identification procedures. Then the fourth section presents the numerical and experimental results of standard measurements and I-E test. Finally, these results are compared to validate the presented method and identify its limits.

Description of Materials

The validation method for the present work was based on the study of commercial silicone rubbers that were formulated from Bluestar Silicones (Lyon, France) products: Bluesil® RTV 3040 and Silbione® HC2/2011. The use of synthetic materials instead of real vascular tissues obtained *post mortem* avoided fast degradation of the latter, so that the comparison of different measurements obtained at different time-points remained relevant. Two materials were formulated: the first material was only composed of RTV 3040, and the second material was a 3040:HC2 mixture, with a 25:75 ratio, called 3040-HC2/75. These materials present different mechanical behaviors within a range typical for vascular walls [8] so that they can be used to produce patient-specific aorta phantoms. Specimens were prepared using the following procedure: (i) mixing the two liquid components, i.e., the uncured silicone and the curing agent, with a 10:1 and 1:1 ratio for RTV 3040 and HC2/2011 respectively, (ii) for 3040-HC2/75 material, mixing the RTV 3040 and HC2/2011 with a 25:75 ratio (iii) putting the uncured mixture into a syringe for centrifugation (5 min at 5000 rpm), in order to eliminate undesired trapped bubbles, (iv) injecting the liquid mixture into molds, plates for the tensile and compression test and in a specific tubular system for I-E tests, and (v) heating molds at 150 °C for 1 h to crosslink the silicone.

Constitutive Models

All the mechanical data are considered in isothermal conditions at ambient temperature. In the literature, several constitutive models have been used to describe vascular wall motion according to various assumptions (anisotropy, orthotropy, incompressibility). These assumptions can be based on the physical description of the vessels (form of collagen fibers, length of elastin) [3, 23, 24] but they generally result in very sophisticated models. More simply, some phenomenological models in use describe the overall mechanical behavior [25, 26]. In the present work, this type of constitutive equation was chosen to limit the number of adjustable parameters, while keeping the best possible description of the behavior. Therefore, a hyper-viscoelastic model, namely a generalized Maxwell solid model, was selected. In this model, the function ψ that

describes the free-energy variation of a transformation in isochoric and isothermal conditions is given by [27]:

$$\psi(\boldsymbol{C}) = \psi_{iso}^{\infty}(\boldsymbol{C}) + \sum_{\alpha=1}^{m} \psi_{\alpha}(\boldsymbol{C}), \tag{1}$$

where $\psi_{iso}^{\infty}(\boldsymbol{C})$ is the strain-energy function characterizing the equilibrium state of the solid represented by the isolated spring, $\boldsymbol{C}$ the right Cauchy-Green strain tensor and m the number of relaxation times. The left-side term of equation (1) represents the hyperelastic behavior and can be experimentally assessed by a sufficiently slow deformation process. For this hyperelastic branch, a Yeoh equation [28] was used, representing an ideal elastic behavior with a nonlinear stress–strain relationship derived from a strain energy density function, which is expressed by:

$$\psi_{iso}^{\infty}(\mathbf{C}) = \sum_{i=1}^{n} C_i (I_1 - 3)^i, \tag{2}$$

with ψ_{iso}^{∞} being the hyperelastic potential, C_i the hyperelastic parameters, I_1 the first invariant of $\mathbf{C}$ ($I_1 = tr(\mathbf{C})$), and n the order of the Yeoh model. This part of the model is able to accurately predict possible hardening encountered in the mechanical response of vascular walls [29, 26] or filled elastomers [27] as occurs in many silicones.

The right-hand term in equation (1), $\sum_{\alpha=1}^{m} \psi_{\alpha}(\boldsymbol{C})$, is the dissipative potential. It represents the viscoelastic contribution and is a function of $\mathbf{C}$. It is straightforward to show that the PK2 (second Piola-Kirchhoff) stress tensor $\mathbf{S}$ is composed of the equilibrium isochoric part $\mathbf{S}_{iso}^{\infty}$ and the non-equilibrium part $\mathbf{Q}_{\alpha}$, $\alpha = 1, \ldots, m$:

$$\mathbf{S} = \mathbf{S}_{iso}^{\infty} + \sum_{\alpha=1}^{m} \mathbf{Q}_{\alpha} . \tag{3}$$

The strain free-energy function responsible for the relaxation with relaxation times τ_{α} is expressed as $\psi_{\alpha}(\mathbf{C}) = \beta_{\alpha} \psi_{iso}^{\infty}(\mathbf{C})$ and its corresponding stress tensor is expressed relative to the equilibrium isochoric part:

$$\mathbf{S}_{iso,\alpha} = \beta_{\alpha} \mathbf{S}_{iso}^{\infty} , \tag{4}$$

where β_{α} is a dimensionless factor.

Then, for each Maxwell element, a linear evolution equation can be considered:

$$\dot{\mathbf{Q}}_{\alpha} + \frac{\mathbf{Q}_{\alpha}}{\tau_{\alpha}} = \dot{\mathbf{S}}_{iso,\alpha} . \tag{5}$$

Moreover, equation (5) can be turned into a convolution integral form giving:

$$\mathbf{Q}_{\alpha} = \int_{-\infty}^{T} e^{-\left(\frac{T-t}{\tau_{\alpha}}\right)} \dot{\mathbf{S}}_{iso,\alpha}(t) dt . \tag{6}$$

In this equation, the entire strain history is taken into account via the time derivative of the stress tensor isochoric part $\dot{\mathbf{S}}_{iso,\alpha}$.

Experimental Mechanical Setup

The number of material parameters (C_i, τ_{α}, β_{α}) to be determined for both the hyperelastic and viscoelastic components of the constitutive model can lead to ill-posed problems [30] if certain precautions are not taken. Therefore, to ensure the reliability of the parameters identified with the I-E test, it is relevant to corroborate their values from other experiments. For this purpose, it is helpful to separate the hyperelastic and viscoelastic behaviors using judiciously chosen tests: the uniaxial tensile test at a very low elongation rate and the dynamic compression test at a low strain value (by Dynamic Mechanical Analysis, DMA).

Tensile and Dynamic Compression Experiments

Tensile test

In order to analyze the hyperelastic behavior of the silicone materials, a CRITERION (MTS Systems, Créteil, France) tensile testing machine equipped with a 500-N load cell was used to perform uniaxial tensile tests. Dumbbell shaped samples approximately 1.5 mm thick were punched out of the previously prepared silicone plates. The initial useful length (l_0) of the samples was 20 mm for a width of 4 mm. The extension was applied up to $\lambda = 1.5$ ($\lambda = l/l_0$) with an extension rate $\dot{\lambda}$ of 5×10^{-3} s^{-1}. This very low extension rate was chosen to prevent any possible viscoelastic effect [31], no hysteresis was observed in these conditions. Moreover, two cyclic tensile tests were previously achieved at the same extension rate in order to detect and erase a possible Mullins effect [32]. The hyperelastic behavior was then analyzed on the third loading curve. Therefore, in the present study, this type of test and the deduced hyperelastic material parameters C_i will be considered as a reference C_i^{ref}. For a uniaxial stress transformation, the right Cauchy-Green deformation tensor $\mathbf{C}$ is given by:

$$\mathbf{C} = \begin{bmatrix} \lambda_1^2 & 0 & 0 \\ 0 & \lambda_2^2 & 0 \\ 0 & 0 & \lambda_3^2 \end{bmatrix}, \tag{7}$$

where λ_1, λ_2 and λ_3 are the principal stretches (with the stretching direction corresponding to the subscript 3) such that, for an isotropic and incompressible material $\lambda_1 = \lambda_2$ and $\lambda_1 \lambda_2 \lambda_3 = 1$.

The Yeoh model applied for such a tensile test leads to the following expression of the corresponding component of the second Piola Kirchoff stress tensor S_{33}:

$$S_{33} = \sum_{i=1}^{n} \frac{iC_i}{\lambda_3^2}\left(2\lambda_3^2 - \frac{2}{\lambda_3}\right)\left(\lambda_3^2 + \frac{2}{\lambda_3} - 3\right)^{i-1} \quad (8)$$

The identification procedure (9) consisted in minimizing the objective function f_{obj}^{h} that measures the gap between the measured stress and the computed one.

$$\left\{C_i^{ref}\Big|i=1\ldots n\right\} = \arg\,minf_{obj}^{h}\left(C_i\Big|i=1\ldots n\right), \quad (9)$$

with f_{obj}^{h} defined as:

$$f_{obj}^{h} = \sum_{j}^{N}\left(S_{33,\,j} - S_{33,j}^{mes}\right)^2, \quad (10)$$

where $S_{33,j}^{mes} = \sigma_{33,j}^{mes} \times \lambda_3^{-2}$ is the second Piola Kirchoff uniaxial stress obtained from the measured tensile true stress $\sigma_{33,j}^{mes}$ and $S_{33,j}$ is the one computed with hyperelastic parameters (Equation (8)), N is the number of measurements taken during the loading process. The optimization procedure was performed by using the optimization toolbox of Matlab software (The MathWorks, Natick, MA, USA) with the trust region reflective optimization algorithm [33].

Compression test

The viscoelastic behaviors of the silicone materials were characterized by frequency sweep experiments in dynamic mechanical analysis in compression mode. These experiments were conducted with a DMA Q800 device (TA Instruments, Guyancourt, France) using disk-shaped samples about 1.5 mm thick (diameter, 7 mm for RTV 3040 and 11 mm for 3040-HC2/75). Dynamic compression test was performed with an angular frequency ω range of 0.06 to 600 rad/s at a constant strain of 1.5 %, which is within the linear viscoelastic regime. For the dynamic compression tests, the silicone material underwent a periodical mechanical strain ε of very small amplitude ε_0 and of angular frequency ω:

$$\varepsilon = \varepsilon_0 \sin(\omega t) \quad (11)$$

From the periodical stress measurement and its phase lag with regard to the strain, the material's complex Young modulus $E^*(\omega)$ was obtained as a function of the angular frequency ω. In the case of the generalized Maxwell model, the storage $E'(\omega)$ and loss $E''(\omega)$ parts of the complex modulus are expressed by equations (12) and (13):

$$E'(\omega) = E_0\left[1 + \sum_{\alpha=1}^{m}\frac{\beta_\alpha\omega^2\tau_\alpha^2}{1 + \omega^2\tau_\alpha^2}\right], \quad (12)$$

$$E''(\omega) = E_0\sum_{\alpha=1}^{m}\frac{\beta_\alpha\omega\tau_\alpha}{1 + \omega^2\tau_\alpha^2}, \quad (13)$$

where E_0 is the Young modulus of the isolated spring. The relaxation times, τ_α, and the dimensionless parameters β_α stand for the contribution of each branch to the total stress. The relaxation time values were fixed regularly spaced between the reciprocals of the highest and the lowest frequencies of the experimental dynamic modulus. The chosen number of modes was sufficiently high to obtain accurate fitting, but not too large to avoid inconsistent results (e.g., negative values of β_α). Practically speaking, this led to five time constants ($m = 5$), regularly spaced on a logarithmic scale between 3×10^{-3} s and 30 s. In the present study, this type of test and the deduced viscoelastic material parameters (E_0, β_α) will be considered as a reference (E_0^{ref}, β_α^{ref}). Identification was achieved by solving the following minimization problem (with the same procedure as above):

$$\left\{E_0^{ref},\,\beta_\alpha^{ref}\Big|\alpha = 1,\ldots,m\right\}$$

$$= \arg minf_{obj}^{v}\left(E_0,\,\beta_\alpha\Big|\alpha = 1,\ldots,m\right), \quad (14)$$

with f_{obj}^{v} defined as:

$$f_{obj}^{v} = \sum_{ij}^{N}\left(E_j' - E_{ij}'^{\,mes}\right)^2, \quad (15)$$

where $E_j'^{\,mes}$ is the storage modulus obtained from the measured data and E_j' is that computed with viscoelastic parameters. As it will be shown in the results section, the Taylor series expansion of the Yeoh model shows that Young modulus E_0 should be six times C_1 [34].

Inflation-Extension Test

The I-E test was developed to simulate as faithfully as possible the deformation of a blood vessel when it is subjected to pulsating flow. Moreover, the device was designed to be coupled with stereovision or non-invasive medical imaging methods (MRI, CT or US) to assist in the calibration of these methods. In the present work, the deformation of the samples was followed using Antares US system (Siemens Healthcare, Saint-Denis, France), for reasons of its low cost and relatively high spatio-temporal resolution (15 μm, 26Hz). However, the use of other imaging methods will be discussed further on the basis of the results obtained.

The silicone tube-shaped sample (internal diameter = 20 mm, thickness = 1.5 mm and length = 100 mm) was positioned in a closed flow circuit (Fig. 1), in which a continuous or pulsed flow can be generated by a pump driven by a command device that can regulate the volume flow rate to simulate the diastole and systole times. This part constitutes the
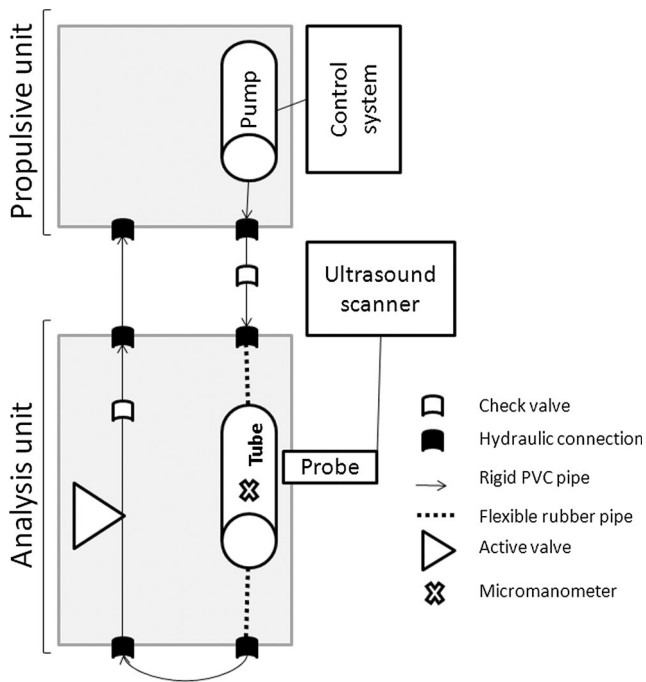
Fig. 1 Inflation-Extension test: The silicone sample tube is placed in the analysis unit in series with the propulsive unit, which is filled with water. Hydraulic connections and rigid PVC pipe are used to ensure an impermeable flow circulation between the two units. Flexible rubber pipes are connected to the ends of the sample tube to avoid circumferential and longitudinal prestreches. The pressure in the sample is driven by a pulsated hydraulic circulation (closed circulation), which is controlled by a submersible pump and its control system. The pressure and elongation recording are measured by a micromanometer placed in the hydraulic circulation inside the tube (using the active valve) and by a US scanner, respectively. Check valves are positioned both upstream and downstream of the tube in order to subtract a possible fluid hammer

propulsive unit. The silicone tube under test was connected to a hydraulic connection with flexible rubber pipes in order to avoid circumferential and longitudinal prestreches. The sample was placed in an analysis unit filled with water in order to carry out US image-based measurements. These two units were connected together by a rigid PVC pipe and rapid connections presenting low regular and low singular pressure losses. Check valves were placed at the input and the output of the tube to avoid a flow back to the pump during the diastole time. The pressure loss coefficient K for these check valves was evaluated ($K=2.0\pm0.2$) [35]. In order to assess the stress components, an accurate determination of the internal pressure synchronized with the deformation measurements is required. The pressure was measured at a sampling frequency of 100 Hz using a 7-F micromanometer-tip catheter (Millar Instruments, Houston, TX, USA) positioned in the tube.

With the objective of simultaneously following the circumferential $\lambda_\theta(t)$ and longitudinal $\lambda_z(t)$ elongations, a linear 38 mm US probe operating at 5 MHz was placed lengthwise with regard to the tube. If this probe was placed in the tube width direction, the circumferential elongation would have

been measured with higher accuracy but the longitudinal elongation could not have been determined. The images from the US scanner clearly depicted the inner and outer boundaries of the silicone tube due to the change of the wave speed between the silicone and water environments with a speed of sound close to 1000 and 1540 m.s^{-1}, respectively. However, there is no natural contrasting marker that could be used for λ_z tracking, neither along the tube wall nor in its thickness (Fig. 2(a)). In the absence of such markers, only the displacements perpendicular to the boundaries (and thus the circumferential elongations λ_θ) can be estimated, which is well known in image processing as the aperture problem. A first solution might be the incorporation of scatterers in the silicone formulation so as to create speckle similar to that observed in the images of tissues. However, the high density of such scatterers necessary to achieve this effect was likely to alter the mechanical behavior of material. Therefore, markers (strips approximately 2 mm thick) were stuck onto the tube surface in the circumferential direction (Fig. 2(b)) to make the longitudinal elongation measurement possible. These markers were sufficiently compliant to avoid any perturbation of the deformation.

After acquisition, each picture of the kinematics data was interactively analyzed using the creaContours[1] software, part of the CreaTools [36] platform to recover the elongation evolution as a function of time. To identify the model parameters, the thickness, the internal diameter and the distance between the two markers need to be quantified, with minimum effort on the part of the user. Furthermore, the low amplitude of the inflation movement justifies a simple assumption that interfaces can be considered rectilinear and parallel to each other. Consequently, it is sufficient to click on two points, a and b, simultaneously defining the first boundary and the distance between the markers, and two other points, c and d, located on the second and third boundaries, respectively (Fig. 3). Then the software builds the line $x=(ab)$, its parallels x' through c, and x'' through d. The line y, perpendicular to x, x' and x'', passes through d, so that $x \cap y = \{b'\}$ and $x' \cap y' = \{c'\}$. Subsequently, the internal diameter $D = \overline{c'd}$, the tube wall thickness $h = \overline{b'c'}$ and the length between the markers $l = \overline{ab}$ are calculated. From these data, the circumferential and longitudinal elongations as a function of time were deduced. It is noteworthy that, in the case of a large number of image sequences acquired, automatic software called Carolab [37, 38], which has already been applied in clinical imaging, could be adapted to estimate these elongations.

In the present study, the I-E test was used in static and dynamic modes. The static mode consisted in applying a continuous flow at constant pressure for 30 s before recording the pressure and elongations. Hence, the measurement only

---

[1] http://www.creatis.insa-lyon.fr/site/fr/CreatoolsCreaContours

Fig. 2 Silicone tube visualization from US imaging: without (**a**) and with (**b**) longitudinal markers; blue lines define the first to third boundaries from *top* to *bottom* for each picture

(a)   (b)
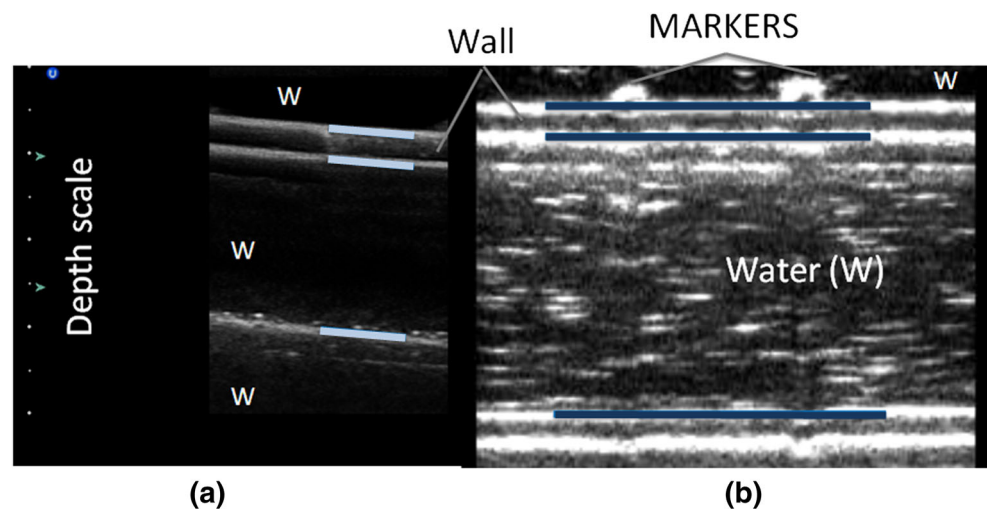
contained the hyperelastic part of the behavior. Here, the imposed static pressure was chosen in a magnitude range (0 to 160 mmHg) consistent with that of a human aorta. For the material 3040-HC2/75, this range was reduced (0 to 75 mmHg) in order to stick to the circumferential elongation physiological range (λ_θ <1.3). In the dynamic mode, a pulsed flow was imposed and, after 30 s, the pressure and elongations were recorded as a function of time. It must be added that, apart from the results presented in the present paper, the transient case was considered and it was verified that the stress pulsation calculated with the parameter sets obtained for the two materials was stabilized after six to eight cycles. Therefore, a delay of 30 s was ample to assume that the discontinuity at the beginning of the strain is sufficiently old so that it does not interfere in the stress evaluation. In these conditions, the steady state can then be used, which can be repeated to give an average over several cycles (we actually averaged five load–unload cycles) and thus increase the signal-to-noise ratio (Fig. 4) In this way, the calculation can be made using equation (6), as though the measured strain pulsation started from minus infinity. The amplitude of the imposed pressure pulsation was chosen in a large magnitude range

bounded by the physiological limit values (P < 160 mmHg and λ_θ <1.3). For the RTV 3040 material, the pressure range was $P \in [2;160]$ mmHg and for the 3040-HC2/75 material $P \in [18;48]$ mmHg. The pulsation rate was approximately 65 pulsations per minute.

However, it was not possible to fully ensure the accurate synchronization of the two signal acquisitions (pressure and US imaging), because of totally independent acquisition devices. Nevertheless, this synchronization must not be ignored because the phase lag between both periodical signals of deformation and stress is characteristic of the viscous behavior. Thus, the synchronization of the curves was performed simultaneously with the adjustment of the parameters to guarantee the consistency of the results. For that purpose, a trial-and-error method was applied. As a starting point, the time origins of the signals were set in such a way that the maxima of the deformation and the pressure coincided, as though the material was purely elastic. Then, a first parameter fitting was performed. If the value of the resulting viscosity was non-zero, a time lag was inevitably obtained between the maxima of the experimental stress and the stress calculated with this first parameter set. The time origin of the experimental stress was

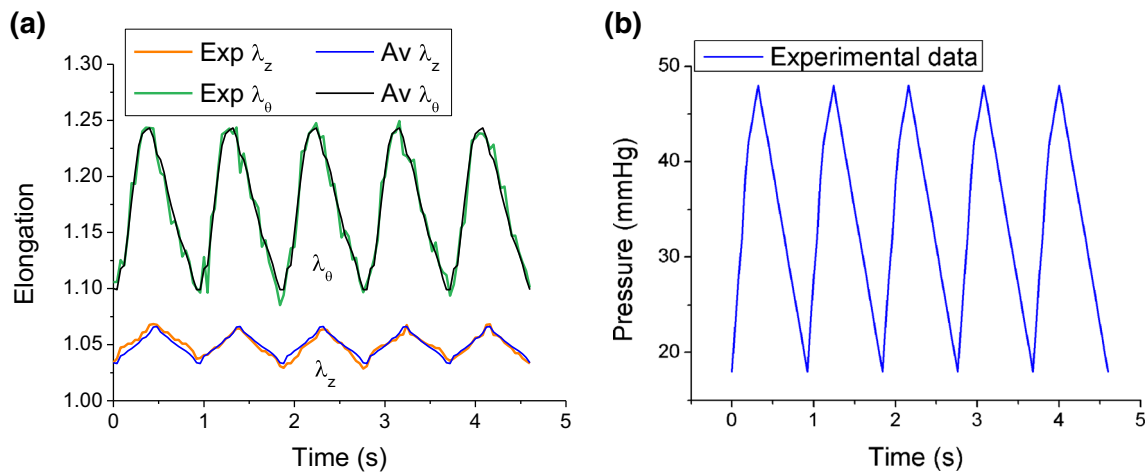**Fig. 3** Computation method for inflation-extension test
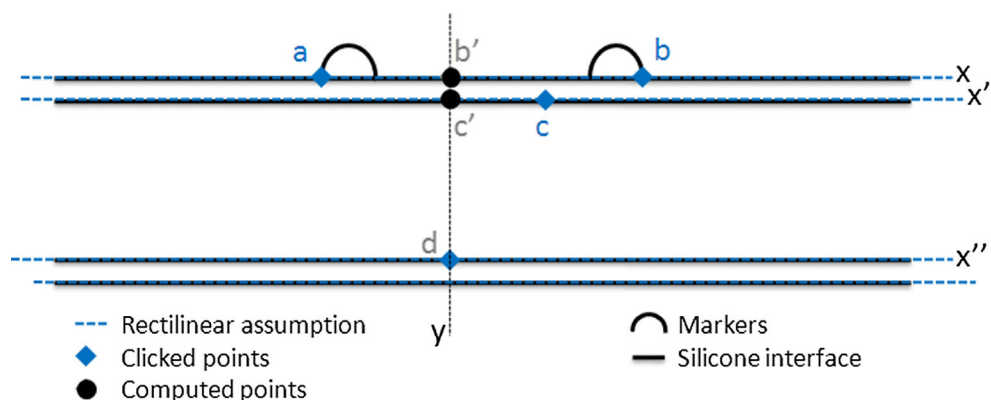
Fig. 4 Elongations (**a**) and pressure (**b**) tracking for 3040-HC2/75 material: Exp (experimental data); Av (Average). The Av *curves* have been obtained by: first, averaging the five cycles of measurements (Exp) represented in this figure, and then, repeatedly tracing the same average cycle

shifted to compensate this time lag, and the parameters were fitted for a second time. This led to a second time lag (smaller than the first one) and the origin of the time scale was again corrected accordingly. This procedure was repeated till the obtained time lag became insignificant, that is, smaller than the sampling time of the experimental signal. Hence, the signals were synchronized in that sense that the stress calculated with the fitted parameters exhibited a maximum at the same position as the experimental one.

Inflation-extension parameters

For the I-E test, cylindrical coordinates are much more appropriate to express the strain. For a tube dilation, the strain expression has been reviewed in detail by [14]. The right Cauchy-Green tensor is written:

$$\boldsymbol{C} = \begin{bmatrix} \lambda_r^2 & 0 & 0 \\ 0 & \lambda_\theta^2 & \gamma\lambda_\theta\lambda_z \\ 0 & \gamma\lambda_\theta\lambda_z & \lambda_z^2(1+\gamma^2) \end{bmatrix}, \tag{16}$$

where λ_r, λ_θ and λ_z are the radial, circumferential and longitudinal elongations, respectively. For an incompressible material, $\lambda_r\lambda_\theta\lambda_z = 1$ so that $\lambda_r = (\lambda_\theta\lambda_z)^{-1}$. The parameter γ is a term associated with the twist angle of the tube arising from the possible bending or torsion of the tube. In this study, for rectilinear parts, this can be ignored ($\gamma = 0$). To define the mechanical behavior of the sample, it is necessary to simultaneously record the circumferential (λ_θ) and longitudinal (λ_z) elongations and the internal pressure $P(t)$ as a function of time. The circumferential elongation is obtained from the diameter measurement:

$$\lambda_\theta = \frac{D(t)}{D(t=0)}, \tag{17}$$

where $D(t=0)$ and $D(t)$ are the internal diameter at the reference and current states, respectively.

The longitudinal elongation is given by equation (18):

$$\lambda_z = \frac{l(t)}{l(t=0)}, \tag{18}$$

where $l(t=0)$ and $l(t)$ are the distances between the markers also at the reference and current states, respectively.

Moreover, as mentioned in the experimental part, the internal pressure is directly measured. For a thick wall, the circumferential stress σ_θ induced by this internal pressure is expressed through equation (19):

$$\sigma_\theta(t) = \frac{(D(t)+h)P}{2h}, \tag{19}$$

where h is the thickness of the tube wall.

The circumferential component of the PK2 stress tensor $S_{iso,\theta}^\infty$ for the hyperelastic part on the constitutive model can be written:

$$S_{iso,\theta}^\infty = \frac{1}{\lambda_\theta}\frac{\partial\psi_{iso}^\infty}{\partial\lambda_\theta} = \lambda_\theta^{-2}\sigma_{iso,\theta}^\infty, \tag{20}$$

where $\sigma_{iso,\theta}^\infty$ is the equilibrium Cauchy stress component. It must be noted that, because of the first invariant I_1 that appears in equation (2), the knowledge of both λ_z and λ_θ is required to determine $\sigma_{iso,\theta}^\infty$.

Then the expression of the total PK2 stress can be obtained from equations (3) and (6). Nevertheless, because of the integral equation including the time derivative of $S_{iso,\theta}^\infty$ in equation (6), some numerical precautions must be taken for this calculation. Consequently, $S_{iso,\theta}^\infty$ can be rewritten using equations (2) and (20) giving:

$$S_{iso,\theta}^\infty = \sum_{i=1}^n C_i \frac{i}{\lambda_\theta}\frac{\partial I_1}{\partial\lambda_\theta}(I_1-3)^{i-1}. \tag{21}$$

At this step, for the assessment of the integration in equation (6), it is judicious to expand the terms of equation (21) into Fourier series [17]. For instance, for a second-order Yeoh model, this leads to the series:

$$\frac{1}{\lambda_\theta}\frac{\partial I_1}{\partial \lambda_\theta} = a_0 + \sum_{k=0}^{p} a_k \cos(k\omega t) + b_k \sin(k\omega t) , \quad (22)$$

$$\frac{2}{\lambda_\theta}\frac{\partial I_1}{\partial \lambda_\theta}(I_1 - 3) = a'_0 + \sum_{k=0}^{p} a'_k \cos(k\omega t) + b'_k \sin(k\omega t). \quad (23)$$

Thus, the time derivative of $S_{iso,\theta}^{\infty}$ is given by:

$$\dot{S}_{iso,\theta}^{\infty} = C_1 \left[\sum_{k=0}^{p} -k\omega a_k \sin(k\omega t) + k\omega b_k \cos(k\omega t) \right]$$
$$+ C_2 \left[\sum_{k=0}^{p} -k\omega a'_k \sin(k\omega t) + k\omega b'_k \cos(k\omega t) \right] . \quad (24)$$

Consequently, equation (6) can present a closed-form expression because it is composed exclusively of products of exponential and sine or cosine functions, as shown in Fig. 5 for the 3040-HC2/75 material. This can be very helpful to avoid numerical integrations that may be blurred because of a relatively poor signal-to-noise ratio or time resolution.

From I-E test, the identification of hyper-viscoelastic material parameters (C_i^{IE}, β_α^{IE}) was performed by solving the minimization problem (using the same procedure as above):

$$\left\{ C_i^{IE}, \beta_\alpha^{IE} \middle| i = 1, ..., n ; \alpha = 1, ..., m \right\}$$
$$= \text{arg} \min f_{obj}^{IE} \left(C_i, \beta_\alpha \middle| i = 1, ..., n ; \alpha = 1, ..., m \right) \quad (25)$$
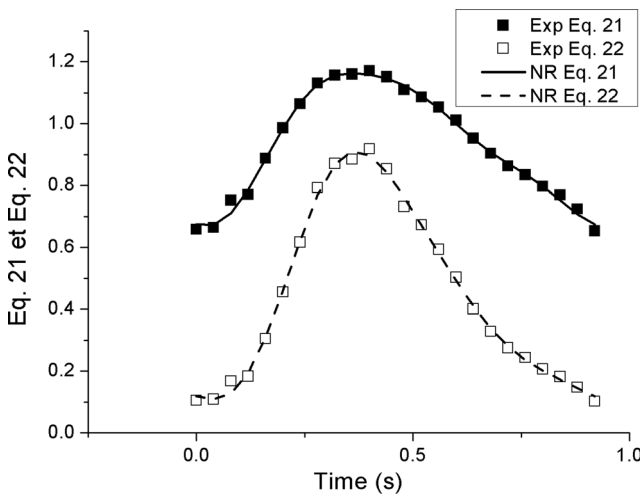

Fig. 5 Modeling results for equations (21 & 22) with third order Fourier series: Exp (experimental data); NR (numerical output data)

with f_{obj}^{IE} defined as:

$$f_{obj}^{IE}\left(C_i, \beta_\alpha \middle| i = 1, ..., n ; \alpha = 1, ..., m \right)$$
$$= \sum_{j}^{N} \left(S_{\theta,j} - S_{\theta,j}^{mes} \right)^2 , \quad (26)$$

where $S_{\theta,i}^{mes}$ is the second Piola Kirchoff measured circumferential stress and $S_{\theta,i}$ is the one computed with hyper-viscoelastic parameters. Theoretically, from the pressure data, both circumferential (S_θ) and longitudinal (S_z) stresses can be expressed. Thus, it could be foreseen to use both of them in the minimization procedure. Besides, the calculation of these stresses requires both circumferential and longitudinal elongations (λ_θ and λ_z). Nevertheless, the longitudinal stress is much more sensitive to λ_z than the circumferential one and the accuracy of the longitudinal elongation measurement is most likely much poorer than this of the circumferential one (see Fig. 4(a)). Therefore, it appeared more convenient to use only the circumferential stress in the minimization procedure.

Results

Reference Parameter Identification from Standard Measurements

From uniaxial tensile and dynamic compression tests, the reference parameters were identified. First, for the two silicone materials studied, RTV 3040 and 3040-HC2/75, uniaxial tensile tests were performed, and the parameters of the Yeoh model were obtained from the stretching curves. As shown by the linear plots of the Cauchy stress versus $\left(\lambda^2 - 1/\lambda \right)$ in Fig. 6-a, a simple first-order Yeoh model, which is reduced to the Neo-Hookean model, is adequate to correctly describe the behavior for the two materials studied. Indeed, non-zero values were obtained for the parameters C_1^{ref} (Table 1), whereas all the other $C_{i\geq2}^{ref}$ were negligible. The agreement between the calculated and experimental results is also shown in Fig. 6(a).

Considering the viscoelastic behavior, the experimental storage moduli $E'(\omega)$ were fitted with equation (12). The contributions (β_α) and the modulus (E_0) were then adjusted. The agreement between the calculated and experimental storage modulus $E'(\omega)$ is shown in Fig. 6(b) and the results obtained are displayed in Table 1. However, each isolated relaxation time does not present a physical meaning when these are imposed. Thus, for the comparison of the two materials' behaviors, it is worth showing an overall viscosity value (η_0) obtained by:

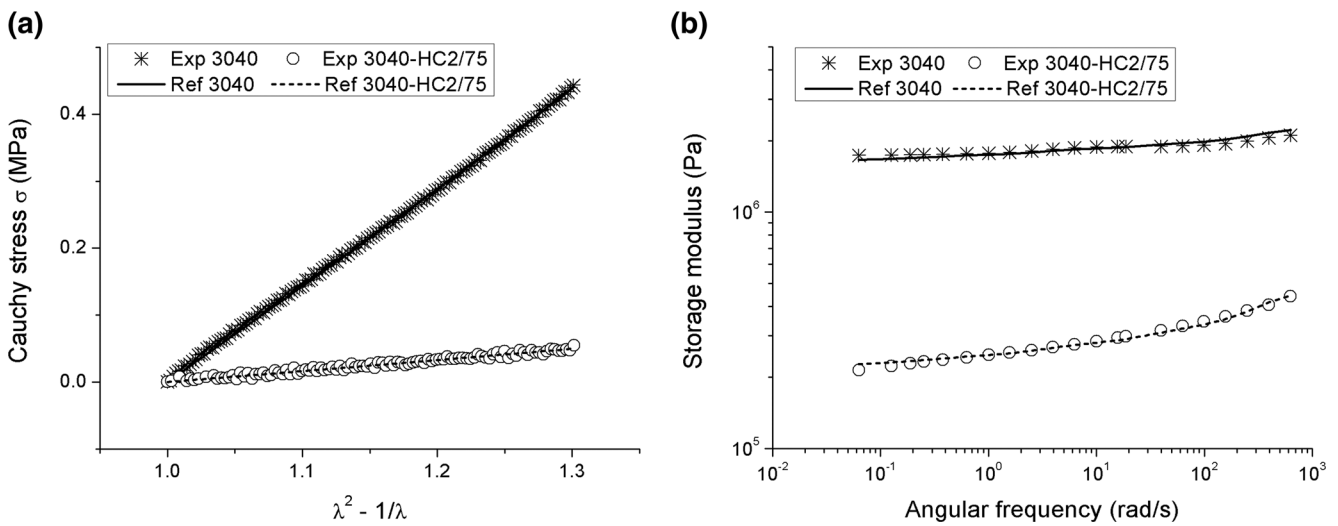$$\eta_0 = \sum_{\alpha=0}^{m} E_0 \beta_\alpha \tau_\alpha . \quad (27)$$

Fig. 6 **a** Uniaxial tensile tests, **b** DMA compression tests: Exp (experimental data), Ref (numerical output data with reference parameters)

In Table 1, the uncertainty of the parameters was obtained from two different experiments for each formulation. It can be mentioned that the obtained parameters for the present silicones compare very well with some values given in the literature for actual aortas. For example, Astrand et al. [3] obtained stiffness values (analogous to C_1) varying from 0.02 to 0.28 MPa according to the age. This confirms that the mechanical properties of the used silicone formulations are representative of the behaviors of actual aortas. Unfortunately, concerning the viscoelastic part, it is more difficult to find quantitative results of relaxation times in the literature to compare them with our results.

Identification of the Parameters from the I-E Test

Hyperelasticity

The results for the two materials, in static mode, are shown in Fig. 7 comparing the experimental points (Exp) and the curves calculated using the reference C_1^{ref} parameters (Ref), and those identified from the I-E test (IE-S). We observe that the C_1^{IE-S} parameters obtained, given in Table 2, are very close to the reference C_1^{ref} (see the second column in Table 1) obtained from tensile tests. Here, the uncertainty of the parameters was calculated on the basis of the uncertainty of the elongation measured from the US images.

This also shows that, for the two materials tested, a simple first-order Yeoh model (i.e., Neo-Hookean) is adequate to describe the hyperelastic behavior, the other constants $C_{i\geq 2}^{ref}$ being null. These preliminary results open the way to investigating the reliability of the I-E measurements in dynamic mode to extract the whole parameter set.

Hyper-viscoelasticity

In the second step, the hyper-viscoelastic behavior was analyzed on the basis of the I-E dynamic mode experiments (see Experimental Mechanical Setup section). Here the numerical input curves (Ref) are those calculated with the reference parameters resulting from the compression test, whereas the numerical output curves (IE-D) were calculated with the parameters identified from the dynamic I-E test data.

Figures 8 and 9 show the respective results for the RTV 3040 and 3040-HC2/75 materials. These stress curves are displayed together with the measured stress as a function of both time (to highlight the time shift) and strain (to highlight the dissipation hysteresis, while hiding the time notion). Taking into account the fact that the reference parameters were obtained from totally independent measurements, the agreement of the corresponding calculated and experimental curves is rather good. Moreover, after fitting, the simulated curves are very close to the experimental ones. This shows that, by

Table 1 Hyperelastic and viscoelastic parameters identified from tensile and DMA tests

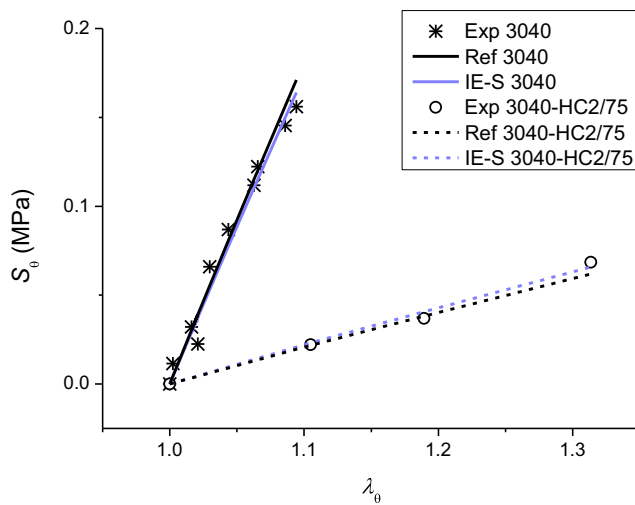| am	C_1^{ref} (MPa)	E_0^{ref} (MPa) $\approx 6.C_1^{ref}$	$\tau_1 = 0.003$ s β_1^{ref}	$\tau_2 = 0.03$ s β_2^{ref}	$\tau_3 = 0.3$ s β_3^{ref}	$\tau_4 = 3$ s β_4^{ref}	$\tau_5 = 30$ s β_5^{ref}	η_0^{ref} (MPa.s)
RTV 3040	0.230±0.006	1.58±0.04	0.215±0.015	0.0892±0.0178	0.0758±0.0085	0.0472±0.0007	0.0481±0.016	2.53±0.70
3040-HC2/75	0.0265±0.0008	0.215±0.020	0.691±0.155	0.222±0.002	0.143±0.006	0.0751±0.0055	0.0636±0.0182	0.469±0.117

Fig. 7 Inflation-extension test for hyperelastic modeling: experimental and computed true stress: Exp (experimental data); IE-S (numerical output data adjusted to the experimental data); Ref (numerical input data from uniaxial tensile test)

nature, the used model is also able to account for the material behavior in the loading mode of the I-E test.

For the two materials, the calculated parameters are displayed in Table 3. Here the uncertainty of the parameters was estimated from different sets of measurements on five cycles. The reverse calculation of the storage modulus curves, using the parameter sets deduced from the I-E measurements (IE-D) is shown in Fig. 10.

Discussion

The values obtained for C_1^{IE-S} and C_1^{IE-D} are very close to those obtained from uniaxial tensile test (C_1^{ref}), which confirms the consistency between all the evaluation methods. Concerning the values of the β_α parameters, as was already mentioned, it is more judicious to compare the values of the overall viscosities (η_0) than each contribution one by one. We observe that only the viscosity of 3040-HC2/75 material was reasonably evaluated (0.675 MPa.s to be compared with 0.469 MPa.s).

For the RTV 3040 material, this overall viscosity is different compared to reference parameters (Table 1). Indeed, a zero value of the viscosity was calculated from the I-E test. Obviously, we meet the limit of I-E test to accurately identify the viscoelastic part of global mechanical behavior. This limit

is partly related to the uncertainties of circumferential and longitudinal elongation measurements by US sonography (1 %), but mainly to the restricted frequency range reachable by the test. Indeed, the pulsation period imposed on the tube (0.92 s) corresponds to the lower bound of the angular frequency around 6 rad/s and the temporal resolution between two images (0.04 s) corresponds to the upper bound of the angular frequency, taking into account the Shannon's theorem, around 80 rad/s. Additionally, the identification of the viscous component of the material becomes less accurate when the elastic modulus is large, since the (hyper)elastic component then tends to hide the viscous component. This observation can be illustrated on the storage modulus curve (Fig. 10) which exhibits a very low variation in the explored angular frequency range. In other words, if the storage modulus is nearly constant, it will be difficult to separate the viscoelastic and hyperelastic parts with the I-E test. Anyway, seeing the circumferential stress-stretch curve (Fig. 8(b)), where the hysteresis is not clearly observed, it would be unrealistic to expect an accurate identification of the viscosity in this case.

More generally, it must be mentioned that the global viscosity calculated is given just as an indicator but it is controversial to rely on this only value to estimate the quality of the results because it can be sensitive to the initial choice of the fixed relaxation times. A further development of the method would be to reconsider this choice regarding the frequency range accessible with the I-E test. The quality of the results is more easily appreciable in the comparison of the calculations in Figs. 8 to 10 where the calculated curves with the different parameters sets are relatively close of the experimental results.

The results of 3040-HC2/75 material are more encouraging: the experimental data show a significant hysteresis (Fig. 9(b)) and the elastic part is low, so it was possible here to identify a value of overall viscosity relatively close to the reference. The relaxation of this material appears clearly in a frequency range more compatible with the sampling time used in the I-E test.

From all these results, several conclusions can be drawn. First, despite the limitations previously noted, the presented I-E test was shown to be efficient in determining the behavior of the materials studied, which are representative of healthy or aneurysmal arterial tissues. Moreover, these results highlight that US imaging can provide relatively accurate information, opening the doors to the possible parameter identification of a blood vessel by *in vivo* measurements. Indeed, the hyper-viscoelastic behaviors of the silicone formulations tested are close to those of the aortic tissue (healthy and pathological). In this respect, it is worth recalling that the actual tissues behaviors can cover a very large range depending on the patient age and health and even on the location of the tissue along the aorta. The proposed method thus appears sufficiently accurate to distinguish these behaviors. This makes it possible to

Table 2 Hyperelastic parameters identified from I-E measurements (static mode)

Silicone	C_1^{IE-S} (MPa)
3040	0.223±0.003
3040-HC2/75	0.0281±0.0006

Fig. 8 Inflation-extension test for hyper-viscoelastic modeling on RTV 3040: **a** stress versus time; **b** stress versus circumferential elongation: Exp (experimental data), IE-D (numerical output data), Ref (numerical input data with reference parameters)
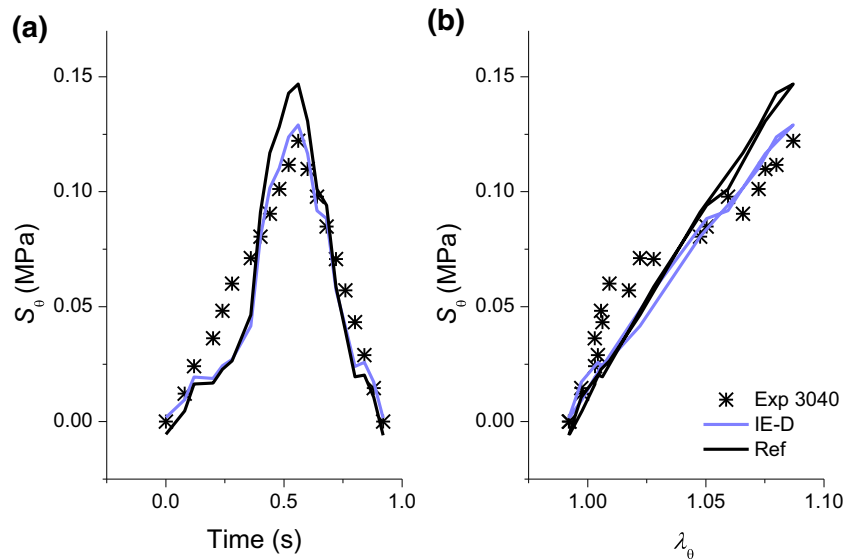
consider minimally invasive measurements and the modeling of hyper-viscoelastic behaviors that could be achieved directly from image acquisition using a US scanner or another imaging technique.

From a practical point of view, the method to identify the hyper-viscoelastic model parameters requires three conditions to be verified in clinical application: the temporal tracking of λ_θ and λ_z with sufficient time resolution, the measurement of the pressure in the region of interest in the aorta, and the synchronization of the two acquisitions.

Depending on the medical imaging modality used, the spatial and temporal resolutions are different. For the present work, the silicone tube motion was visualized by ultrasound imaging. However, in the absence of scatterers within the material, natural landmarks that could be used in λ_z tracking

are missing. This problem was solved by adding physical markers on the tube. It was then shown that both spatial and temporal resolutions of this imaging technique (15 μm and 26 Hz, respectively) are sufficient to identify the hyper-viscoelastic parameters. However, in the case of actual clinical tests, it is obviously impossible to use this type of marker. Fortunately, it has been shown by performing US imaging on blood vessels such as carotid arteries that some organic elements (elastin, collagen, extracellular matrix, etc.) in the arterial layers, act as scatterers. Hence, a "speckle" texture is generated, which can be advantageously used for λ_z tracking. Nevertheless, for deep vessels like the aorta tree, it may be more difficult to use this technique because of a coarser spatial resolution achieved when the probe frequency is decreased to obtain a deeper penetration, and physical obstacles such as the

Fig. 9 Inflation-extension test for hyper-viscoelastic modeling on 3040-HC2/75: **a** stress versus time; **b** stress versus circumferential elongation: Exp (experimental data), IE-D (numerical output data), Ref (numerical input data with reference parameters)
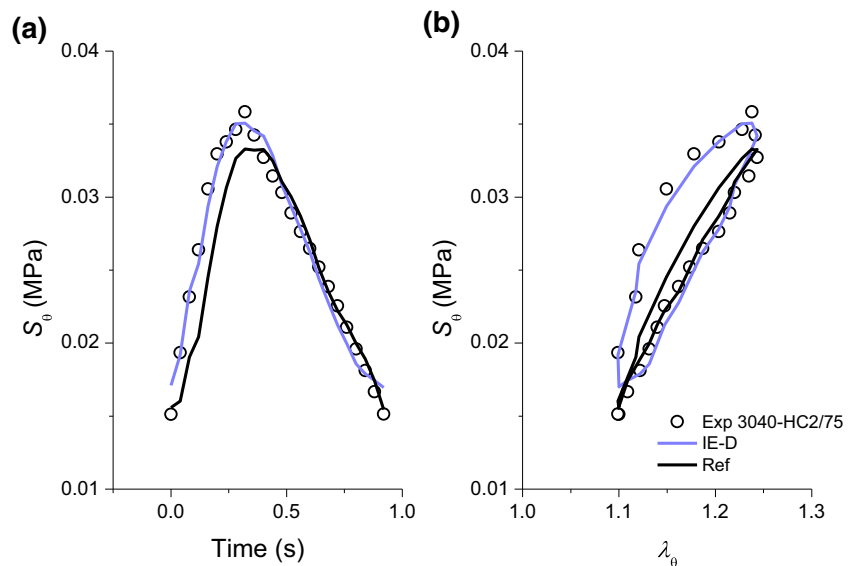
Table 3 Hyper-viscoelastic parameters identified from I-E measurements (dynamic mode)

Silicone	C_1^{IE-D} (MPa)	$\tau_1 = 0.003$ s β_1^{IE-D}	$\tau_2 = 0.03$ s β_2^{IE-D}	$\tau_3 = 0.3$ s β_3^{IE-D}	$\tau_4 = 3$ s β_4^{IE-D}	$\tau_5 = 30$ s β_5^{IE-D}	η_0^{IE-D} (MPa.s)
RTV 3040	0.220±0.004	–	–	–	–	–	0
3040-HC2/75	0.0273±0.0001	–	1.06±0.15	0.339±0.004	–	0.133±0.030	0.675±0.149

ribs. The use of other imaging techniques, such as MRI or CT, might be considered. However, in CT, image acquisition is performed with a relatively low temporal resolution close to 4 Hz, which is not enough for the purposes of this study (only four measurements per cycle would be possible). Furthermore, this imaging technique involves X-ray radiation and might require an iodine contrast agent in the blood to observe the arterial lumen and it would be difficult to define longitudinal landmarks. Conversely, current sequences used in MRI give a higher temporal resolution close to 20Hz. Nevertheless, in dynamic physiological conditions, this technique demonstrates poor spatial resolution (about 1 mm).

Rigorously speaking, the simultaneous measurement of the blood pressure to assess stress is required to model hyperviscoelastic behavior. At present, this only can be performed using a micromanometer placed within the region of interest in the aorta. As percutaneous introducing of a micromanometer is invasive, such a procedure would have to take advantage of the catheter used for coronarography in the cases where the latter is performed prior to surgery. Otherwise, blood pressure could be non-invasively measured in another part of the body, as a recent study [39] has obtained encouraging results in estimating local pressure variations via indirect measurements. Anyway, non-synchronization of the pressure and deformation measurements must be taken into account to evaluate the model parameters as long as integrated synchronizing solution is not implemented by scanner vendors. For this purpose, the procedure proposed in this work can be used.

Conclusion

The aim of this study was to validate an identification method using an inflation-extension measurement on a tube, in order to accurately predict the mechanical behavior of its wall in terms of both hyperelastic and viscoelastic components. Such a system can be used as a helpful tool for the development of aorta phantoms with a behavior as realistic as possible. The method was validated by showing that the hyper-viscoelastic behaviors of silicone materials, having properties similar to the aorta, were successfully identified and compared well with the standard measurements (tensile tests and DMA). Ultrasound imaging was able to track elongations throughout the dynamic solicitation of cylindrical samples. The use of the present method in the clinical environment for *in vivo* experiments using common imaging techniques can be foreseen provided precautions are taken in terms of spatio-temporal resolution and signal synchronization. Eventually, the methodology developed to identify the model parameters would be helpful to predict vascular pathologies from *in vivo* experiments considering the alteration of the tissue behavior due to the disease.
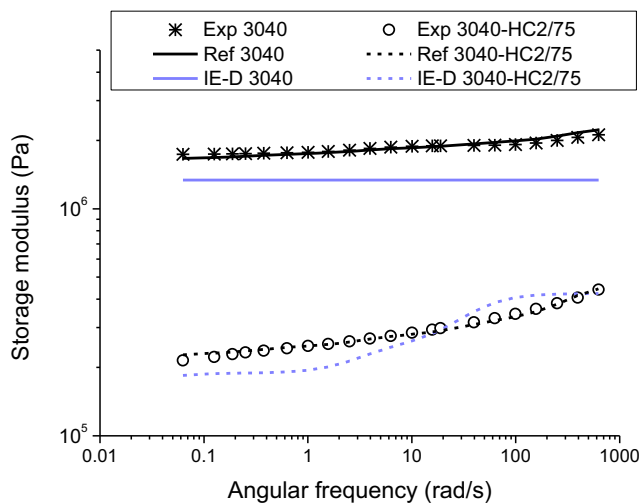
Fig. 10 DMA compression experiments and curves calculated from I-E results: Exp (experimental data), Ref (numerical output data), IE-D (numerical input data from the I-E test)

References

1. Long A, Rouet L, Bissery A, Rossignol P, Mouradian D, Sapoval M (2005) Compliance of abdominal aortic aneurysms evaluated by tissue Doppler imaging: correlation with aneurysm size. J Vasc Surg 42(1):18–26. doi:10.1016/j.jvs.2005.03.037
2. Riley WA, Barnes RW, Evans GW, Burke GL (1992) Ultrasonic measurement of the elastic modulus of the common carotid artery. The atherosclerosis risk in communities (ARIC) study. Stroke 23(7):952–956. doi:10.1161/01.str.23.7.952

3. Astrand H, Stalhand J, Karlsson J, Karlsson M, Sonesson B, Lanne T (2011) *In vivo* estimation of the contribution of elastin and collagen to the mechanical properties in the human abdominal aorta: effect of age and sex. J Appl Physiol 110(1):176–187

4. Wilson KA, Lindholt JS, Hoskins PR, Heickendorff L, Vammen S, Bradbury AW (2001) The relationship between abdominal aortic aneurysm distensibility and serum markers of elastin and collagen metabolism. Eur J Vasc Endovasc Surg 21(2):175–178

5. Konig G, McAllister TN, Dusserre N, Garrido SA, Iyican C, Marini A, Fiorillo A, Avila H, Wystrychowski W, Zagalski K, Maruszewski M, Jones AL, Cierpka L, de la Fuente LM, L'Heureux N (2009) Mechanical properties of completely autologous human tissue engineered blood vessels compared to human saphenous vein and mammary artery. Biomaterials 30(8):1542–1550. doi:10.1016/j.biomaterials.2008.11.011

6. Corbett TJ, Doyle BJ, Callanan A, Walsh MT, McGloughlin TM (2010) Engineering silicone rubbers for *in vitro* studies: creating AAA models and ILT analogues with physiological properties. J Biomech Eng 132(1):011008. doi:10.1115/1.4000156

7. Shimamura J, Kubota H, Endo H, Tsuchiya H, Kawashima N, Sudo K (2012) Three-dimensional replica of a life-sized model of aortic arch aneurysm for preoperative assessments. Ann Thorac Surg 93(5):1699–1702. doi:10.1016/j.athoracsur.2012.01.072

8. Sulaiman A, Boussel L, Taconnet F, Serfaty JM, Alsaid H, Attia C, Huet L, Douek P (2008) *In vitro* non-rigid life-size model of aortic arch aneurysm for endovascular prosthesis assessment. Eur J Cardio-Thoracic Surg: Off J Eur Assoc Cardio-Thoracic Surg 33(1):53–57. doi:10.1016/j.ejcts.2007.10.016

9. van't Veer M, Buth J, Merkx M, Tonino P, van den Bosch H, Pijls N, van de Vosse F (2008) Biomechanical properties of abdominal aortic aneurysms assessed by simultaneously measured pressure and volume changes in humans. J Vasc Surg 48(6):1401–1407. doi:10.1016/j.jvs.2008.06.060

10. Molacek J, Baxa J, Houdek K, Treska V, Ferda J (2011) Assessment of abdominal aortic aneurysm wall distensibility with electrocardiography-gated computed tomography. Ann Vasc Surg 25(8):1036–1042

11. Astrand H, Ryden-Ahlgren A, Sandgren T, Lanne T (2005) Age-related increase in wall stress of the human abdominal aorta: an *in vivo* study. J Vasc Surg 42(5):926–931. doi:10.1016/j.jvs.2005.07.010

12. Redheuil A, Yu WC, Wu CO, Mousseaux E, de Cesare A, Yan R, Kachenoura N, Bluemke D, Lima JA (2010) Reduced ascending aortic strain and distensibility: earliest manifestations of vascular aging in humans. Hypertension 55(2):319–326. doi:10.1161/hypertensionaha.109.141275

13. Li L, Qian X, Yan S, Hua L, Zhang H, Liu Z (2012) Determination of the material parameters of four-fibre family model based on uniaxial extension data of arterial walls. Comp Methods Biomech Biomed Eng. doi:10.1080/10255842.2012.714374

14. Holzapfel G, Gasser T, Ogden R (2000) A new constitutive framework for arterial wall mechanics and a comparative study of material models. J Elast 61(1):1–48

15. Holzapfel GA, Gasser TC, Stadler M (2002) A structural model for the viscoelastic behavior of arterial walls: continuum formulation and finite element analysis. Eur J Mech A/Solids 21(3):441–463

16. Valdez-Jasso D, Bia D, Haider MA, Zocalo Y, Armentano RL, Olufsen MS (2010) Linear and nonlinear viscoelastic modeling of ovine aortic biomechanical properties under *in vivo* and *ex vivo* conditions. Conf Proc: Annu Int Conf IEEE Eng Med Biol Soc IEEE Eng Med Biol Soc Conf 2010:2634–2637. doi:10.1109/iembs.2010.5626563

17. Zhang W, Liu Y, Kassab GS (2007) Viscoelasticity reduces the dynamic stresses and strains in the vessel wall: implications for vessel fatigue. Am J Physiol Heart Circ Physiol 293(4):H2355–H2360. doi:10.1152/ajpheart.00423.2007

18. van Dam EA, Dams SD, Peters GW, Rutten MC, Schurink GW, Buth J, van de Vosse FN (2008) Non-linear viscoelastic behavior of abdominal aortic aneurysm thrombus. Biomech Model Mechanobiol 7(2):127–137. doi:10.1007/s10237-007-0080-3

19. Bell V, Mitchell WA, Sigurðsson S, Westenberg JJM, Gotal JD, Torjesen AA, Aspelund T, Launer LJ, de Roos A, Gudnason V, Harris TB, Mitchell GF (2014) Longitudinal and circumferential strain of the proximal aorta. J Am Heart Assoc 3 (6). doi:10.1161/jaha.114.001536

20. Chong CK, How TV, Harris PL (2005) Flow visualization in a model of a bifurcated stent-graft. J Endovasc Ther 12(4):435–445. doi:10.1583/04-1465.1

21. Gulan U, Luthi B, Holzner M, Liberzon A, Tsinober A, Kinzelbach W (2014) Experimental investigation of the influence of the aortic stiffness on hemodynamics in the ascending aorta. IEEE J Biomed Health Inf. doi:10.1109/jbhi.2014.2322934

22. Anssari-Benam A, Korakianitis T (2013) An experimental model to simulate arterial pulsatile flow: *in vitro* pressure and pressure gradient wave study. Exp Mech 53(4):649–660. doi:10.1007/s11340-012-9675-4

23. Holzapfel GA, Gasser TC (2001) A viscoelastic model for fiber-reinforced composites at finite strains: continuum basis, computational aspects and applications. Comput Methods Appl Mech Eng 190(34):4379–4403

24. Nierenberger M (2013) Multiscale mechanics of vascular walls: Experiments, imaging, modeling. Mécanique des matériaux, Université de Strasbourg

25. Balocco S, Basset O, Courbebaisse G, Boni E, Frangi AF, Tortoli P, Cachard C (2010) Estimation of the viscoelastic properties of vessel walls using a computational model and Doppler ultrasound. Phys Med Biol 55(12):3557–3575. doi:10.1088/0031-9155/55/12/019

26. Courtial E-J (2015) Elaboration of silicone materials with a mechanical behavior tailored for manufacturing patient-specific aortic phantom. University of Claude Bernard Lyon 1

27. Holzapfel GA (2000) Nonlinear solid mechanics: A continuum approach for engineering. Wiley edn

28. Yeoh OH (1993) Some forms of the strain energy function for rubber. Rubber Chem Technol 66(5):754–771. doi:10.5254/1.3538343

29. Vassal J-P, Avril S, Genovese K (2009) Caractérisation des propriétés mécaniques d'un tronçon d'aorte par une méthode inverse basée sur des mesures *ex-vivo* du champ de déformations. Paper presented at the 19ème congrès de mécanique, Marseilles

30. Friedrich C, Honerkamp J, Weese J (1996) New ill-posed problems in rheology. Rheol Acta 35(2):186–193. doi:10.1007/BF00396045

31. Benkahla J, Baranger TN, Issartel J (2012) Experimental and numerical simulation of elastomeric outsole bending. Exp Mech 52(9):1461–1473. doi:10.1007/s11340-012-9606-4

32. Mullins L (1969) Softening of rubber by deformation. Rubber Chem Technol 42(1):339–362. doi:10.5254/1.3539210

33. Sorensen D (1982) Newton's method with a model trust region modification. SIAM J Numer Anal 19(2):409–426. doi:10.1137/0719026

34. Dong Y, Lin RJT, Bhattacharyya D (2005) Determination of critical material parameters for numerical simulation of acrylic sheet forming. J Mater Sci 40(2):399–410. doi:10.1007/s10853-005-6096-0

35. Idel'cik IE (1969) Mémento des pertes de charge, coefficients de pertes de charge singulières et de pertes de charge par frottement, vol 13. vol Collection du Centre de recherches et d'essais de Chatou. Eyrolles

36. Dávila Serrano EE, Guigues L, Roux JP, Cervenansky F, Camarasu-Pop S, Riveros Reyes JG, Flórez Valencia L, Hernández Hoyos M, Orkisz M (2012) CreaTools: applications and development framework for medical image-processing

software. Paper presented at the ISBI Workshop on Open Source Medical Image Analysis Software, Barcelona, Spain, 05/2012

37. Zahnd G, Orkisz M, Serusclat A, Moulin P, Vray D (2013) Evaluation of a Kalman-based block matching method to assess the bi-dimensional motion of the carotid artery wall in B-mode ultrasound sequences. Med Image Anal 17(5):573–585. doi:10.1016/j.media.2013.03.006

38. Zahnd G, Orkisz M, Serusclat A, Moulin P, Vray D (2013) Simultaneous extraction of carotid artery intima-media interfaces in ultrasound images: assessment of wall thickness temporal variation during the cardiac cycle. Int J Comput Assist Radiol Surg. doi:10.1007/s11548-013-0945-0

39. Fazeli N, Kim C-S, Rashedi M, Chappell A, Wang S, MacArthur R, McMurtry MS, Finegan B, Hahn J-O (2014) Subject-specific estimation of central aortic blood pressure via system identification: preliminary in-human experimental study. Med Biol Eng Comput 52(10):895–904. doi:10.1007/s11517-014-1185-3